# Robot Joint Angle Control Based on Self Resonance Cancellation Using Double Encoders

Akiyuki Hasegawa[1], Hiroshi Fujimoto[1] and Taro Takahashi[2]

*Abstract*— Research on the control using a load-side encoder for two-mass system is getting more active due to the widespread use of the load-side encoder. We previously proposed Self Resonance Cancellation, which is a position control method for two-mass system. SRC has steady-state error and the vibration suppression performance is not improved. In the industry, Proportional-Proportional Integral control is commonly used, however, P-PI has problems such that poles can't be arranged arbitrarily and bad performance in the disturbance suppression performance. In this paper, SRC and P-PI combined and complement each other's faults and control performance is improved. In other words, poles can be arranged arbitrarily, the vibration suppression performance and the disturbance suppression performance is improved and the control bandwidth become higher. Simulation and experimental results show the effectiveness of the proposed method.

## I. INTRODUCTION

In the industry, there are many controlled objects that can be modeled into two-mass systems. Hence control of two-mass system is very important in engineering. Robots joints with gears or timing-belt are modeled into two-mass system. Therefore, studies on position control of two-mass system are important for robots control. Conventionally, two-mass system position control method using an observer has been actively studied [1], [2]. However, observers are greatly affected by modeling error of the plants.

In recent years, the load-side encoder has been widely used. It is because that the load-side positioning accuracy has become more required and cost of the load-side encoder has become lower. Therefore, studies on control methods using a load-side encoder has been active [3], [4], [5], [6].

We previously proposed Self Resonance Cancellation (SRC) which is a position control method for two-mass system [7]. Although SRC has the advantage of simplifying controller design, the vibration suppression performance is bad. In the industry, Proportional-Proportional Integral (P-PI) control is commonly used, because its simplicity and comprehensibility are in great demand. However, P-PI has problems such that poles can't be arranged arbitrarily and bad performance in the disturbance suppression. If we use state feedback method, pole arranging arbitrarily is possible. However, parameters of robot joint are change according to posture fluctuation, thus state feedback is not appropriate for robot joint angle control in terms of robustness.

[1]The University of Tokyo, 5-1-5 Kashiwanoha, Kashiwa, Chiba, 277- 8561, Japan, hasegawa16@hflab.k.u-tokyo.ac.jp, fujimoto@k.u-tokyo.ac.jp
[2]Advanced Technology Engineering Department,Partner Robot Division, Toyota Motor Corporation 1-4-18, Koraku, Bunkyo-ku, Tokyo 112-8701, Japan taro_takahashi@mail.toyota.co.jp
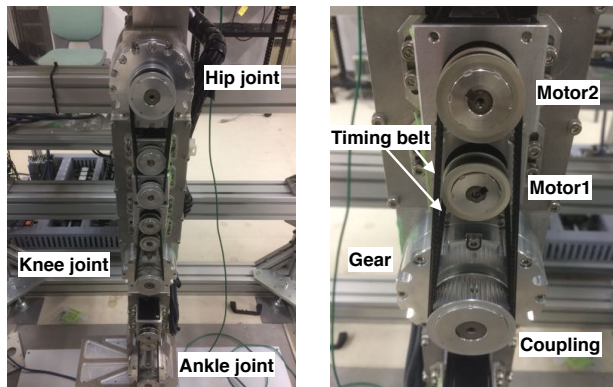
(a) Overview      (b) Knee joint

Fig. 1: Experimental machine of leg robot

In this paper, SRC is combined with P-PI and they complement each other's faults. In other words, the proposed method can arrange poles arbitrarily and has improved control performances.

The purpose of this paper is to propose a method combining simplicity, comprehensibility, improved control performance for robot joint, which is modeled into two-mass system. In section II, experimental setup and modeling is shown. In section III, the design and the principle of the method proposed is described. In section IV, Simulations results and experiments results show the superiority of the proposed method.

## II. EXPERIMENTAL SETUP AND MODELING

### A. Leg Robot

Fig. 1a shows the experimental machine of a leg robot. The robot has a hip joint, a knee joint and an ankle joint. It is possible to measure the characteristics of only the leg, because the waist is fixed by the frame, The knee joint of the leg robot is shown in Fig. 1b.

As shown in the Fig. 1b, the leg robot joint consists of two motors and belts. This structure enables us to downsize motors and to place motors freely, and joints which consists of double motors and belt are proposed for humanoid robot in previous studies [8], [9]. The leg robot employs encoders not only on the motor-side but also on the load-side, so that control methods using information on the load-side can be implemented.

Fig. 2 is a schematic diagram of the joint which is shown in Fig. 1b. $M_1$ and $M_2$ denote the motors, $L$ and $l$ denotes the
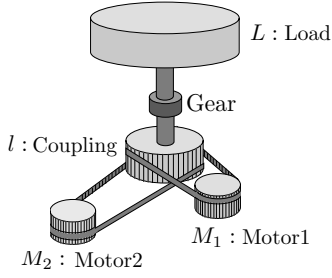
Fig. 2: Schematic diagram of single joint with double encoders

load and the coupling, respectively. The frequency response of the knee joint was measured. Fig. 3 shows the frequency response from the motor1 input torque $T_{M1}$ to the load-side angle $\theta_L$. TABLE I shows modeling parameters. The measurement experiment were conducted using a frequency domain identification method [10] and each joint of the robot legs are in standing posture. Fig. 3 shows the joint has anti-resonances and resonances.

*B. Two-mass Motor Bench*

Robots joints with gears or timing-belt are modeled into two-mass system as shown in Fig. 4a and Fig. 4b. We conducted experiments using two-mass motor bench to show clearly the performance of the control methods. Fig. 5 shows the experimental machine of the two-mass motor bench. It has not only a motor-side motor but a load-side motor, therefore we can add the load-side disturbance or measure the frequency response from the load-side.

Fig. 6 shows the frequency responses of the two-mass motor bench. TABLE II shows modeling parameters.

## III. SRC-P-PI

*A. Self Resonance Cancellation [7]*

Block diagram of SRC system is shown in Fig. 7. Here, $J_{SRC} = J_M + J_L$. SRC calculates virtual angle $\theta_{SRC}$ from the motor-side angle $\theta_M$ and the load-side angle $\theta_L$.

$\theta_{SRC}$ is denoted by (1), and $\theta_{SRC}$ is the center of gravity of the motor-side angle and the load-side angle.
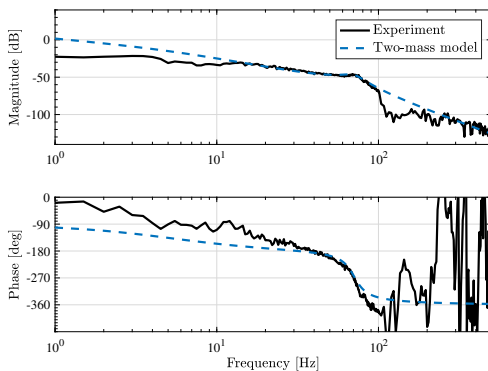


Fig. 3: Frequency response of knee joint. From the motor1 input torque $T_{M1}$ to the load-side angle $\theta_L$.
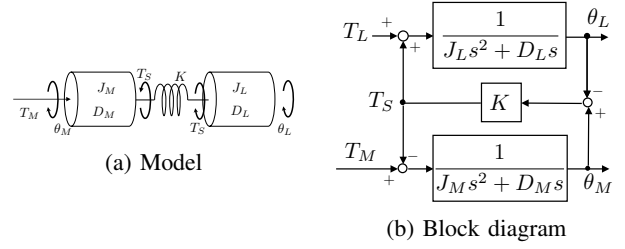


(a) Model



(b) Block diagram

Fig. 4: Two-mass system



Fig. 5: Experimental machine of two-mass motor bench

$$\theta_{SRC} = \frac{J_M}{J_M + J_L}\theta_M + \frac{J_L}{J_M + J_L}\theta_L. \quad (1)$$

The equation of motion on the motor-side and the load-side in the inertial system is denoted by (2), (3), therefore $\ddot{\theta}_{SRC}$ is denoted by (4).

$$J_M\ddot{\theta}_M = T_M - K(\theta_M - \theta_L), \quad (2)$$

$$J_L\ddot{\theta}_L = K(\theta_M - \theta_L), \quad (3)$$

$$\ddot{\theta}_{SRC} = \frac{J_M\ddot{\theta}_M}{J_M + J_L} + \frac{J_L\ddot{\theta}_L}{J_M + J_L}$$

$$= \frac{T_M}{J_M + J_L}. \quad (4)$$

TABLE I: Parameter of leg robot knee joint

| | | | |
|---|---|---|---|
| $J_{M1}$ | Motor1-side moment of inertia | 8.31e-6 | kg m$^2$/s$^2$ |
| $J_{M2}$ | Motor2-side moment of inertia | 8.31e-6 | kg m$^2$/s$^2$ |
| $J_l$ | Coupling moment of inertia | 1e-6 | kg m$^2$/s$^2$ |
| $J_L$ | Load-side moment of inertia | 0.25 | kg m$^2$/s$^2$ |
| $D_{M1}$ | Motor1-side viscosity friction coefficient | 2e-3 | kg m/s |
| $D_{M2}$ | Motor2-side viscosity friction coefficient | 2e-3 | kg m/s |
| $D_l$ | Coupling viscosity friction coefficient | 2e-3 | kg m/s |
| $D_L$ | Load-side viscosity friction coefficient | 10 | kg m/s |
| $K_1$ | Belt1 torsional rigidity coefficient | 120.5 | kg m/s$^2$ |
| $K_2$ | Belt2 torsional rigidity coefficient | 100.5 | kg m/s$^2$ |
| $K_L$ | Harmonic gear torsional rigidity coefficient | 2.3e+4 | kg m/s$^2$ |
| $r_p$ | Gear ratio of belt | 1.71 | |
| $r_h$ | Gear ratio of harmonic gear | 50 | |
| $K_T$ | Torque constant | 0.327 | N / Arms |

TABLE II: Parameter of two-mass motor bench

| | | | |
|---|---|---|---|
| $J_M$ | Motor-side moment of inertia | 0.0019 | kg m$^2$/s$^2$ |
| $J_L$ | Load-side moment of inertia | 0.0057 | kg m$^2$/s$^2$ |
| $D_M$ | Motor-side viscosity friction coefficient | 0.0018 | kg m/s |
| $D_L$ | Load-side viscosity friction coefficient | 0.0826 | kg m/s |
| $K$ | Torsional rigidity coefficient | 93.6137 | kg m/s$^2$ |
| $r$ | Gear ratio | 1 | |
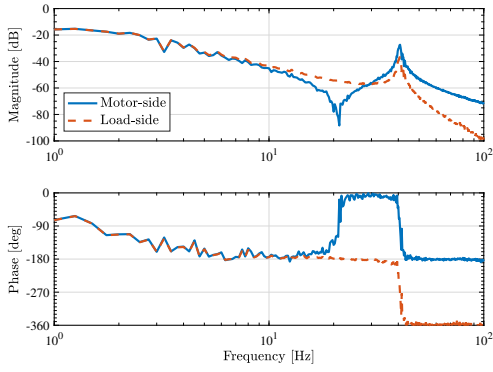
Fig. 6: Frequency response of two-mass motor bench



Fig. 8: Comparison of frequency characteristics of the transfer function from the input torque to the motor-side angle $\frac{\theta_M}{T_M}$ , from the input torque to the load-side angle $\frac{\theta_L}{T_M}$ and from the input torque to the centroid angle $\frac{\theta_{SRC}}{T_M}$

The transfer function from the input torque $T_M$ to the centroid angle $\theta_{SRC}$ is given by

$$\frac{\theta_{SRC}}{T_M} = \frac{1}{(J_M + J_L)s^2}$$
$$= \frac{1}{J_{SRC}s^2}, \quad (5)$$

where $J_{SRC} = J_M + J_L$. The transfer function from the input torque $T_M$ to the centroid angle $\theta_{SRC}$ has no resonance as shown in Fig. 8, therefore feedback of $\theta_{SRC}$ makes control bandwidth higher. In addition to it, the design of the controller becomes very simple, because it is a rigid body model without resonance. However, even if $\theta_{SRC}$ is controlled, the load-side angle $\theta_L$ deviates from the command value. For example, when $\theta_M$ and $\theta_L$ are vibrating, if the amplitudes is the inertia ratio and the frequencies are the same, $\theta_{SRC}$ is a constant value. Also, since $\theta_{SRC}$ neglects the resonance, therefore SRC is difficult to improve vibration suppression performance.
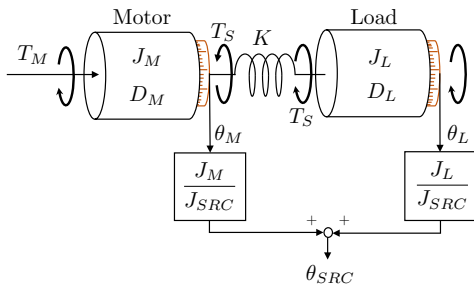


Fig. 7: Block diagram of SRC system [7]

*B. Proportional-Proportional Integral Control (Conventional)*

Block diagram of P-PI is shown in Fig. 9. Inner-loop of P-PI is motor-side angular velocity $\omega_M$ control loop with PI controller and outer-loop of P-PI is the load-side angle $\theta_L$ control loop with P controller. The structure is simple and the relationship between their gains and the control performance is clear. However, P-PI has disadvantages. First, P-PI can't arrange poles arbitrarily, thus hand-tuning of
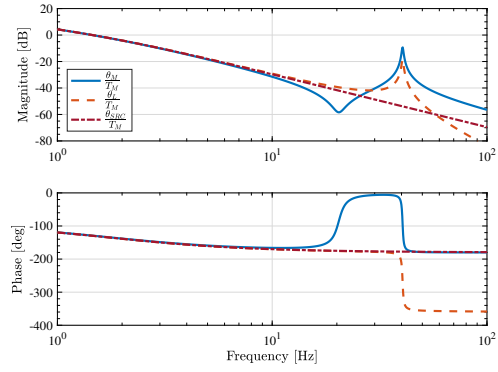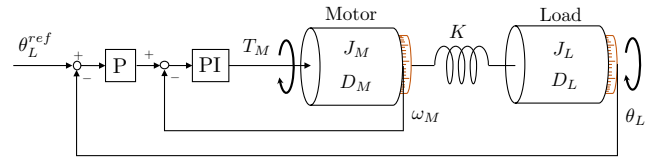


Fig. 9: Block diagram of the P-PI system for angle control

controller gain is needed. Second, the control bandwidth of the inner-loop is limited by the anti-resonance frequency. Third, bad performance in the disturbance suppression.

*C. SRC-P-PI Control (Proposed)*

Even if $\theta_{SRC}$ is feedbacked directly, the load-side angle does not follow the command value. Several solutions have already been proposed for this problem. Previous method solved the problem by eliminating the difference between the load-side angle $\theta_L$ and the centroid angle $\theta_{SRC}$ [4], [5], [6].

In this paper, we propose a control method shown in the block diagram of Fig. 10. In the method proposed, the difference between the load-side angle $\theta_L$ and the centroid angle $\theta_{SRC}$ is not eliminated. Inner-loop of SRC-P-PI is the centroid angular velocity $\omega_{SRC}$ control loop with PI controller and outer-loop of SRC-P-PI is the load-side angle control loop with P controller and all-pass-filter (APF). APF is used as a phase compensation filter.

While P-PI controls the motor-side angular velocity $\omega_M$ in inner-loop, SRC-P-PI controls the centroid angular velocity $\omega_{SRC}$ in inner-loop. (5) showed that the transfer function from the input torque $T_M$ to the centroid angle $\theta_{SRC}$ has no resonance and anti-resonance. As a result, poles of inner-loop can be arranged arbitrarily by the PI controller, and it is possible to design inner-loop with high control bandwidth exceeding resonance and anti-resonance. However, SRC-P-PI neglects the resonance and anti-resonance in the inner-loop, therefore it is necessary to improve the vibration suppression
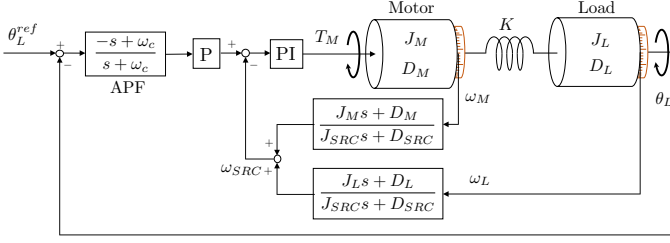
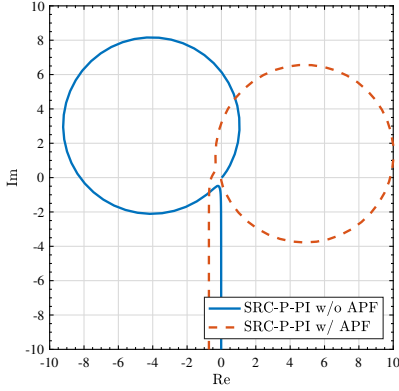Fig. 10: Block diagram of the SRC-P-PI system for angle control



Fig. 11: APF effect in the Nyquist diagram. APF rotate the Nyquist diagram.

performance of the outer-loop. The outer-loop of SRC-P-PI has APF as a phase compensator for vibration suppression. The effect of APF is shown in Fig. 11. APF rotate the Nyquist diagram, therefore the system become stable.

In other words, SRC-P-PI enhances the disturbance suppression performance by making the control bandwidth of the inner-loop higher, and the outer-loop has vibration suppression performance. P-PI has 3 parameters required to be tuned by hand, while SRC-P-PI has 2 parameters (outer P gain and APF cutoff frequency) to be tuned by hand, that is, SRC-P-PI is easier to design than P-PI.
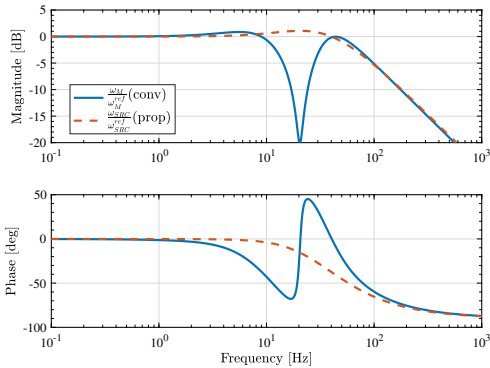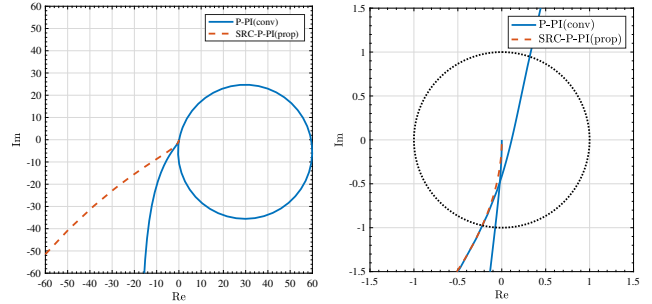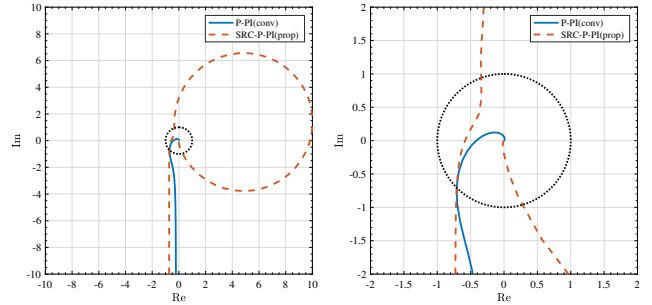


Fig. 12: Bode diagram of inner-loop. Two roll-offs at the high frequencies are aligned in the same form for fair comparison.



(a) Overview (b) Enlarged View

Fig. 13: Inner-loop phase margin. The phase margins are aligned for fair comparison.



(a) Overview (b) Enlarged View

Fig. 14: Inner-loop phase margin. The phase margins are aligned for fair comparison.

In the proposed method the control system is designed as following steps.

1) System Identification
   Identify the motor-side inertia $J_M$ and viscosity friction coefficient $D_M$ and those of load-side $J_L, D_L$.
2) Design SRC and inner loop controller
   We can make SRC with plant parameters $J_M, D_M, J_L, D_L$. The inner loop PI controller are designed for the rigid body $\dfrac{1}{(J_M + J_L)s}$. Poles can be arranged arbitrarily.
3) Design All Pass Filter
   The cut off frequency $\omega_c$ should be a little higher the resonance frequency. We can change the phase margin with APF.
4) Tuning outer loop controller
   The outer loop P controller is tuned by hand.

## IV. SIMULATION

A simulation is conducted using the parameters of the motor bench shown in TABLE II. The resonance frequency $\omega_p$ was around 40 Hz, and the simulation was done in a continuous system. SRC-P-PI system shown in Fig. 10 is compared with P-PI system shown in Fig. 9. Note that SRC-P-PI and P-PI control need two encoders.The purpose of SRC-P-PI system is to obtain better performance with easier tuning parameters.
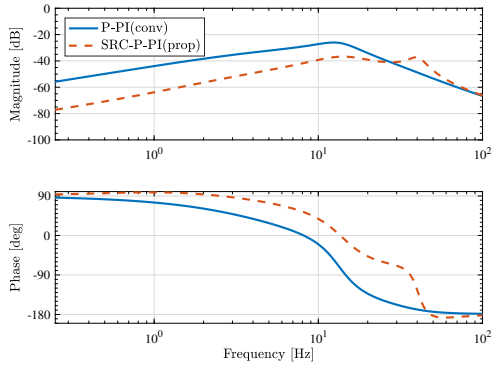
Fig. 15: The sensitivity function from the load-side distur-bance to the load-side angle $\dfrac{\theta_L}{T_L}$ (Simulation)
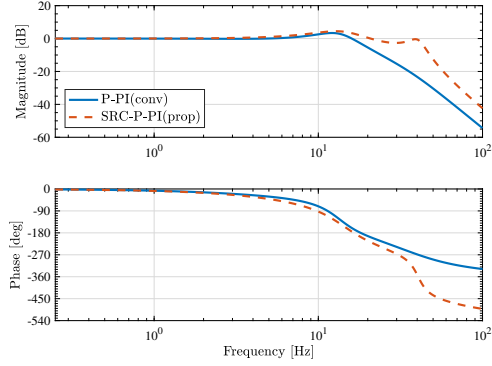


Fig. 16: Bode diagram of outer-loop from the load-side command value to the load side angle $\dfrac{\theta_L}{\theta_L^{ref}}$ (Simulation)
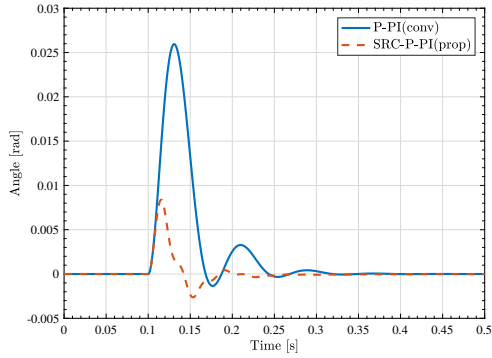


Fig. 17: Time response of load-side angle. Load-side step disturbance was added at $0.1$ s (Simulation)



Fig. 18: The sensitivity function from the load-side distur-bance to the load-side angle $\dfrac{\theta_L}{T_L}$ (Experiment)



Fig. 19: Bode diagram of outer-loop from the load-side command value to the load side angle $\dfrac{\theta_L}{\theta_L^{ref}}$ (Experiment)



Fig. 20: Time response of load-side angle. Load-side step disturbance was added at $0.1$ s (Experiment)

For fair comparison, the control bandwidth and the phase margin of the inner-loop has been adjusted as shown in Fig. 12 and in Fig. 13. The control bandwidth of the two methods are arranged close to 80 Hz. In the inner-loop of the conventional method, it is necessary to design the PI gain by trial and error. On the other hand, SRC-P-PI can set PI gain by poles arrangement, because from the input torque $T_M$ to the centroid angular velocity $\omega_{SRC}$ is rigidified. Also, inner-loop control bandwidth of P-PI can not exceeding the anti-resonance and the resonance frequency, while that of SRC-P-PI can exceeding them. The inner-loop control bandwidth
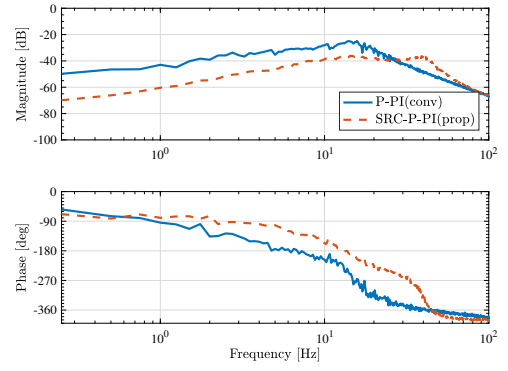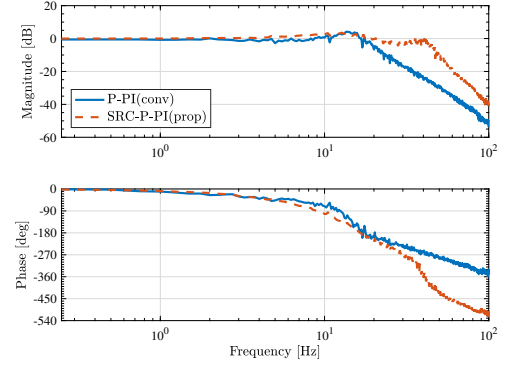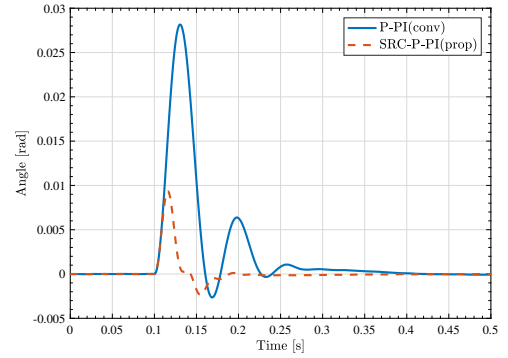
of SRC-P-PI is limited by the rated current of the motor. The P gain of the outer-loop of each method was designed in a trial and error manner so that the phase margin of each method is $45$ degree, as in Fig. 14.

*A. Frequency domain analysis*

Fig. 15 shows the load-side disturbance suppression per-formance. In the low-frequencies, the proposed method has lower gain from the load-side disturbance $T_L$ to the load-side angle $\theta_L$, that is, the proposed method has the better load-side disturbance suppression performance. Higher control

TABLE III: Comparison of performance of SRC-P-PI and P-PI

| | Hand-tuning parameters | Disturbance suppression | Control bandwidth |
|---|---|---|---|
| P-PI | 3 (P, P and I gain) | (standard) | 16 Hz |
| SRC-P-PI | 2 (P and $\omega_c$ of APF) | better | 41 Hz |

bandwidth of inner-loop which exceed the anti-resonance and resonance frequency and feedback $\theta_{SRC}$ including information on the load-side improves the load-side disturbance suppression performance.

We compared the closed-loop frequency characteristics from the command value $\theta_L^{ref}$ to the output $\theta_L$ in Fig. 16. The proposed method has higher control bandwidth than the conventional method.

TABLE III shows the comparison of performance of SRC-P-PI and P-PI. SRC-P-PI is better in both the disturbance suppression performance and the control bandwidth despite the small number of hand-tuning parameters. The control bandwidth is defined at a frequency at which the gain is $-3$ dB.

### B. Time Responses

Fig. 17 shows the simulation result of the load-side step disturbance response. The output is the load-side angle $\theta_L$. The command value $\theta_L^{ref}$ is 0.0 rad. The load-side disturbance force (0.5 N) is added at 0.1 s.

In terms of minimizing the maximum fluctuation of output, the proposed method is better than conventional method. If settling time is defined as the time response curve to reach and stay within a range of $\pm0.001$ rad, the settling time of P-PI is 0.2330 s and that of SRC-P-PI is 0.1654 s. SRC-P-PI settles in less time.

### V. EXPERIMENT

#### A. Frequency domain analysis

We conducted experiments using the motor bench shown in Fig. 5. The experiments conditions are the same as the simulations conditions. The controllers are discretized by Tustin conversion whose sampling frequency is 2.5 kHz. The results of experiments are almost the same as the those of simulations.

Fig. 18 shows the load-side disturbance suppression performance. Since the motor-bench has load-side motor, it is possible to input torque from the load-side. The measurement experiment were conducted using a frequency domain identification method [10].

The proposed method has the better load-side disturbance suppression performance. We compared the closed-loop frequency characteristics from the command value $\theta_L^{ref}$ to the output $\theta_L$ in Fig. 19. The proposed method has higher control bandwidth than the conventional method.

#### B. Time Responses

Fig. 20 shows the experiment result of the load-side step disturbance response. If settling time is defined as the

time response curve to reach and stay within a range of $\pm0.001$ rad, the settling time of P-PI is 0.2616 s and that of SRC-P-PI is 0.1644 s. SRC-P-PI settles in less time.

### VI. CONCLUSION

P-PI system is widely used in the industry as a method using a load-side encoder to control the load-side angle of two-mass system. The proposed method has a similar structure to P-PI control and controls the center-of-gravity angular velocity in the inner-loop. In the proposed method, poles of inner-loop can be arranged arbitrarily by the PI controller, and it is possible to design inner-loop with high control bandwidth exceeding resonance and anti-resonance. As a results, the disturbance suppression performance and the outer-loop control bandwidth of proposed method are superior to that of P-PI. Robots work in environments often receiving external force, therefore the disturbance suppression performance is important. In addition, the number of hand-tuning parameters of the proposed method is one less than that of the P-PI control, that is, the proposed method is easier to design controllers.

### REFERENCES

[1] K. Yuki, T. Murakami, and K. Ohnishi, "Vibration control of a 2 mass resonant system by the resonance ratio control," *IEEJ Transactions on Industry Applications*, vol. 113, no. 10, pp. 1162–1169, 1994.

[2] Y. Hori, "2-mass system control based on load-side acceleration control and state feedback," *IEEJ Transactions on Industry Applications*, vol. 112(5), pp. 499–500, 1992.

[3] E. Saito and S. Katsura, "Vibration control of two-mass resonant system based on wave compensator," *IEEJ Transactions on Industry Applications*, vol. 132, no. 4, pp. 2672–2677, 2011.

[4] M. Aoki, "Robust Resonance Suppression Control based on Self Resonance Cancellation Disturbance Observer and Application to Humanoid Robot," in *2013 IEEE International Conference on Mechatronics (ICM)*, 2013, pp. 623–628.

[5] K. Sakata, H. Asaumi, K. Hirachi, K. Saiki, and H. Fujimoto, "Self Resonance Cancellation Techniques for a Two-Mass System and Its Application to a Large-Scale Stage," *IEEJ Journal of Industry Applications*, vol. 3, no. 6, pp. 455–462, 2014.

[6] S. Yamada, K. Inukai, and H. Fujimoto, "Proposal of Self Resonance Cancellation Control without Using Drive-Side Information," in *Industrial Electronics Society, IECON 2015 - 41st Annual Conference of the IEEE*, 2015, pp. 783–788.

[7] K. Sakata, K. Saiki, and H. Fujimoto, "Self Resonance Cancellation using Multiple Sensors for Ballscrew Driven Stage," in *2011I EE-Japan Industry Application Society Conference (IEEJ JIASC 2011)*, no. 1, 2011, pp. 521–526.

[8] Y. Ito, S. Nozawa, J. Urata, T. Nakaoka, and K. Kobayashi, "Development and Verification of Life-Size Humanoid with High-Output Actuation System," in *2014 IEEE International Conference on Robotics and Automation (ICRA)*, 2014, pp. 3433–3438.

[9] J. L. &. J.-H. O. Ill-Woo Park, Jung-Yup Kim, "Mechanical design of the humanoid robot platform, HUBO," *Advanced Robotics*, vol. 21, no. 11, pp. 1305–1322, 2007.

[10] J. Pitelon, Rik Schoukens, *System Identification: A Frequency Domain Approach, 2nd Editon*. Wiley-IEEE Press, 2012.